analytical chemistry

Article

Cite This: Anal. Chem. 2019, 91, 13237−13243

pubs.acs.org/ac

Highly Luminescent and Self-Enhanced Electrochemiluminescence of Tris(bipyridine) Ruthenium(II) Nanohybrid and Its Sensing Application for Label-Free Detection of MicroRNA

Jing Ye,[†] Guoyong Liu,[†,‡] Mengxia Yan,[†,‡] Qiuju Zhu,[†] Liping Zhu,[†] Jianshe Huang,*[,‡] and Xiurong Yang*[,†,‡]

[†]Department of Chemistry, University of Science and Technology of China, Hefei, Anhui 230026, P. R. China

[‡]State Key Laboratory of Electroanalytical Chemistry, Changchun Institute of Applied Chemistry, Chinese Academy of Sciences, Changchun, Jilin 130022, China

Supporting Information

ABSTRACT: Inspired by the coreactive activity of carbon nanodots (CDs) and branched polyethylenimine (BPEI) toward electrochemiluminescence (ECL) of $Ru(bpy)_3^{2+}$, a highly luminescent and self-enhanced ECL nanohybrid (Ru-BCDs) was synthesized through covalently linking BPEI-coated carbon dots (BCDs) with Tris (4,4′-dicarboxylic acid-2,2′-bipyridyl) ruthenium(II) dichloride ($Ru(dcbpy)_3^{2+}$). The composition and morphological characterization demonstrated that the spherical Ru-BCDs particles with 12.1 ± 1.4 nm diameter were obtained. The enhanced ECL property of Ru-BCDs was proved to originate from the dual coreactive contribution of BPEI and CDs as coreactants as well as the intramolecular electron transfer process, which could shorten the electron transfer path and minimize energy loss. A carbon nitride nanosheet (CNN) was utilized to stabilize the Ru-BCDs-modified glassy carbon electrode, which greatly improved the stability of solid-state ECL. By utilizing the affinity discrepancy of the CNN to single-stranded and double-stranded nucleic acids, a label-free and signal-on ECL biosensor was constructed for the determination of microRNA-133a (miR-133a), a potential biomarker of acute myocardial infarction. The designed biosensor exhibited good performance of miR-133a detection with a detection limit of 60 fM and could be used for the detection of real human serum with satisfactory results. The self-enhanced ECL nanohybrid with distinguished ECL efficiency holds a promising prospect in biosensing and bioimaging applications.

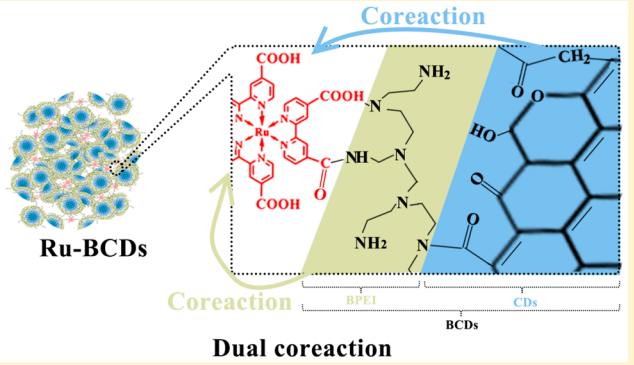

The electrochemiluminescence (ECL) analytical technique, a combination of electrochemistry and chemiluminescence, is valuable for the bioanalytical field because of its rapid response, low background signal, and outstanding sensitivity.[1−3] Traditionally, the ECL system depends on the intermolecular reaction between the luminophore and coreactant via directly adding the coreactant in the testing solution.[4,5] However, the long electronic transmission distance in the intermolecular reaction increases the energy loss, hinders electron transmission, and causes reagent consumption and measurement error.[6,7] On the basis of this consideration, more and more intramolecular ECL reagents are designed to overcome the defects by covalently linking luminophore and coreactant. For example, Sun's group proposed an intramolecular ECL luminophore of ruthenium(II) tris-bipyridyl ($Ru(bpy)_3^{2+}$) derivatives linked to tripropylamine (TPA) through an amide bond for the first time, which achieved a good ECL performance.[8,9] In succession, by replacing volatile TPA with branched poly(ethylenimine) (BPEI), an amine-rich polymeric compound, Yuan's group made considerable works to develop the $Ru(bpy)_3^{2+}$-BPEI complex as a self-enhanced ECL emitter.[10,11] The self-enhanced emitter could overcome the shortcomings of a traditional ECL system and obtain high ECL efficiency with a low concentration of coreactant, even without adding extra coreactant.[12,13]

Recently, it has been reported that carbon nanodots (CDs) also could be used as the coreactive reagent to improve the ECL of $Ru(bpy)_3^{2+}$, whose ECL mechanism was attributed to the benzylic alcohol groups on the surface of CDs.[14] Utilizing the ECL system of $Ru(bpy)_3^{2+}$/CDs in solution, several sensitive sensing platforms have been built to detect Ru-$(bpy)_3^{2+}$,[15] bisphenol A,[16] pentachl orophenol,[17] chlorinated phenols,[18] and so on. Additionally, nitrogen-doped carbon nanodots have also been regarded as the coreactant and carrier

Received: August 13, 2019
Accepted: September 17, 2019
Published: September 17, 2019

DOI: 10.1021/acs.analchem.9b03674
Anal. Chem. 2019, 91, 13237−13243

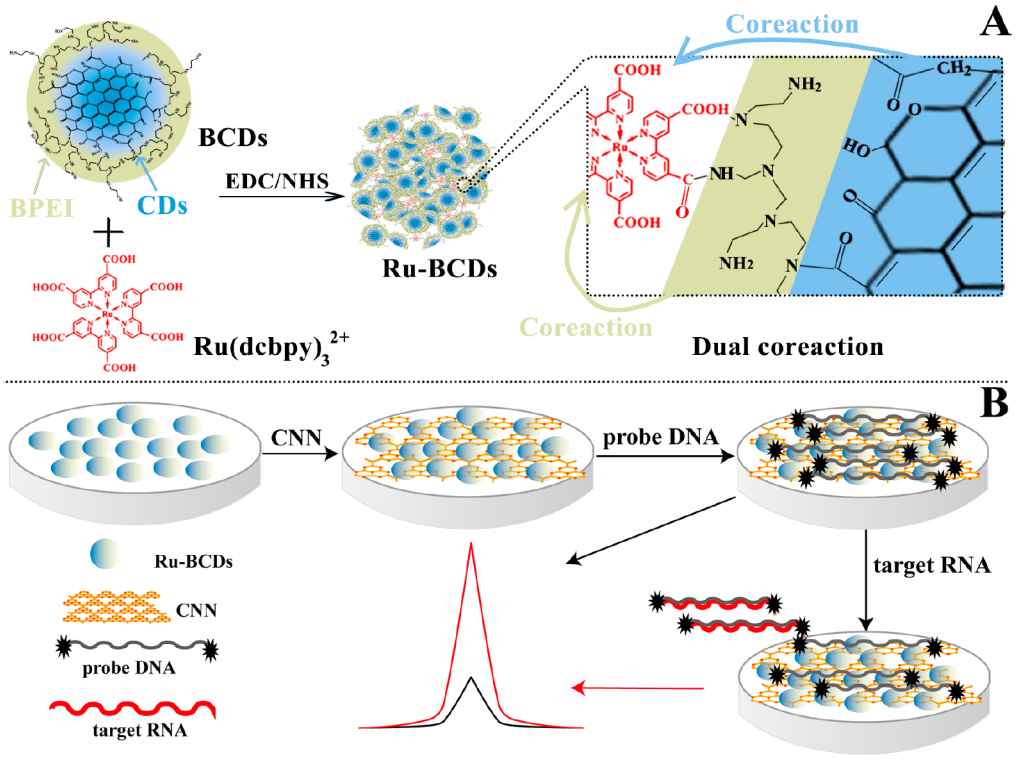

Figure 1. (A) Preparation and possible self-enhanced ECL mechanism of Ru-BCDs nanohybrid. (B) Fabrication process of biosensor.

to prepare self-enhanced ECL labels.[19] Compared with TPA, CDs possess many advantages, such as large specific surface area, low toxicity, eco-friendly properties, and easy functionalization.[20] These intrinsic properties make CDs as one kind of promising alternative to the traditional organic coreactants. Also, the abundant functional groups on CDs enable it to be easily modified to further improve the coreactive ability.

The label-free sensing method has attracted great attention in recent years because this method does not need complicated labeling and purification steps.[21] Many two-dimensional (2D) nanosheets which could interact with DNA have been widely used to build a label-free biosensor, such as graphene oxide,[22] carbon nitride nanosheet (CNN),[23] chalcogenide nanosheet,[24] functionalized h-BN nanosheet,[25] and β-Ni(OH)$_2$ nanosheet.[26] Among them, metal-free CNN shows more considerable potential, because CNN could be prepared through exfoliation from bulk carbon nitride (CN) without the need of surfactants or oxidation treatment.[27,28] For example, Liao et al. designed a label-free fluorescence sensor based on the affinity changes of CNN to single-stranded DNA and double-stranded DNA.[29] Feng et al. used a CNN-modified electrode to load hemin-labeled ss-DNA to prepare an ECL DNA biosensor.[30] These findings demonstrated the CNN-based label-free sensor was a very promising sensing platform.

Considering the above-mentioned studies, we prepared a self-enhanced ECL emitter by means of a covalent linkage between (4,4′-dicarboxylic acid-2,2′-bipyridyl) ruthenium(II) dichloride (Ru(dcbpy)$_3^{2+}$), a poly carboxyl derivative of Ru(bpy)$_3^{2+}$, and BPEI-coated CDs (BCDs), marked as Ru-BCDs (Figure 1A). Because of the dual enhancement contribution from BPEI and CDs to the ECL of Ru(dcbpy)$_3^{2+}$, Ru-BCDs nanohybrid exhibited superior ECL emission without additional coreactant. Therefore, a new label-free solid-state ECL platform was proposed with Ru-BCDs as self-enhanced luminophore and CNN as ss-DNA nanocarrier. MicroRNA-133a (miR-133a), a potential biomarker of acute myocardial infarction (AMI), was selected as a model target. As shown in Figure 1B, the Ru-BCDs nanohybrid was dropped on the glassy carbon electrode (GCE), exhibiting an efficient self-enhanced ECL property. Exfoliated CNN was dropped to stabilize the luminescence of Ru-BCDs in view of the superb film-forming ability.[23,31] Moreover, the ferrocene-labeled single-stranded probe DNA could attach strongly onto the surface of CNN to quench the luminescence of Ru-BCDs. In the presence of miR-133a, the hybridized DNA-RNA complex would weaken the interactions between CNN and bases and fall off from the GCE surface, bringing the recovery of ECL signal. This label-free sensing strategy showed the simple detection of target RNA with excellent selectivity and high stability.

EXPERIMENTAL SECTION

Reagents. Melamine and citric acid (CA) were purchased from Alfa Aesar. Branched polyethylenimine (BPEI, Mw = 1.8 kDa) was obtained from Aladdin (Shanghai, China). Tris (4,4′-dicarboxylic acid-2,2′-bipyridyl) ruthenium(II) dichloride (Ru(dcbpy)$_3^{2+}$) was bought from Suna Tech. Inc. (Suzhou, China). *N*-Hydroxy sulfo-succinimide (NHS), *N*-(3-(dimethylamino)propyl)-*N*′-ethylcarbodiimide hydrochloride (EDC), chloroauric acid, $NaH_2PO_4{\cdot}12H_2O$, and $Na_2HPO_4{\cdot}7H_2O$ were obtained from Sigma-Aldrich (St. Louis, MO). 1-Aminopyrene (AP) was obtained from Acros Organics (New Jersey, U.S.A.). $K_4[Fe(CN)_6]$, $K_3[Fe(CN)_6]$ and KCl were bought from Beijing Chemical Works (Beijing, China). Ultrapure water (18.25 MΩ·cm, Milli-Q, Millipore) was used in all experiments. All DNA and RNA oligonucleotides were purchased from Sangon Biotechnology Co. Ltd. (Shanghai, China), and their sequences are shown as follows.

DOI: 10.1021/acs.analchem.9b03674
Anal. Chem. 2019, 91, 13237−13243

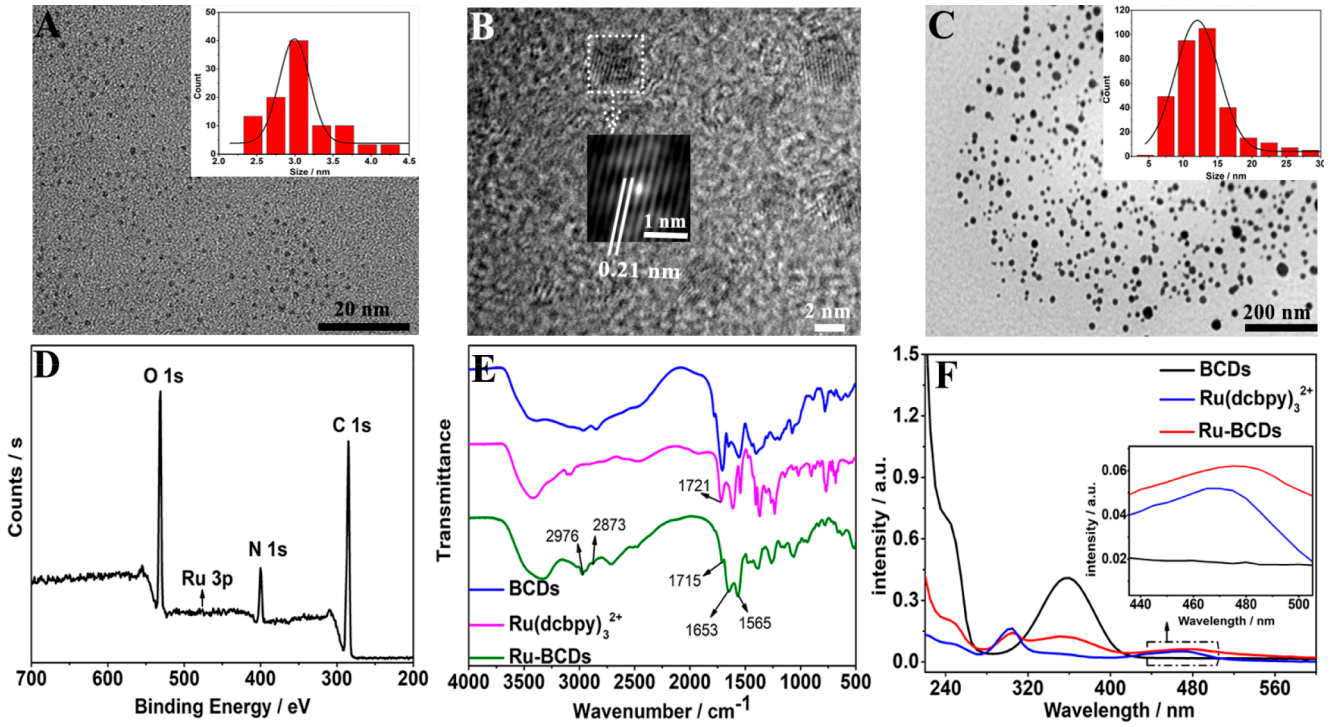

Figure 2. (A) TEM image of BCDs. (B) High-resolution TEM image of BCDs. Inset is the Fourier Transformation image within the dashed line rectangle. (C) TEM image of Ru-BCDs. Insets of (A) and (C) are the corresponding particle size distributions. (D) XPS spectrum of Ru-BCDs. (E) FT-IR spectra and (F) UV−vis absorption spectra of BCDs, $Ru(dcbpy)_3^{2+}$ and Ru-BCDs. Inset of (F) represents the magnification of the dashed line frame.

probe DNA: 5′-Fc-ATTTGGTTCCATTTTACCAGCT-Fc-3′

miR-133a: 5′-AGCUGGUAAAAUGGAACCAAAU-3′

miR-499a: 5′-UUAAGACUUGCAGUGAUGUUU-3′

miR-208b: 5′-AAGCUUUUUGCUCGAAUUAUG U-3′

miR-328: 5′-CUGGCCCUCUCUGCCCUUCCGU-3′

Synthesis of CNN. CNN was synthesized as described previously.[27] In brief, the melamine was heated at 550 °C with the heating rate of 3 °C/min. After heating, the residue was collected and thoroughly ground to obtain the yellowish powder (bulk CN). Twenty milligrams of bulk CN was dispersed in 20 mL of DI water, followed by ultrasonic treatment at 100 W for about 18 h. The formed milk-white solution was centrifuged at 9000 rpm to collect the supernatant CNN solution.

Synthesis of BCDs. The amine-rich BPEI-capped carbon dots (BCDs) were obtained via microwave heating of an aqueous solution of CA and BPEI. Typically, CA (1 g) and BPEI (0.4 g) were successively dissolved in 30 mL of H_2O with ultrasound assistant. The mixture was heated at 700 W for 3 min by domestic microwave oven. The microwave heating process was repeated for 2−3 times. In the process of microwave heating, the solution color changed from transparent to pale-yellow as a result of formation of BCDs. After the solution was allowed to naturally cool to room temperature, it was centrifuged (8000 rpm, 10 min) and washed with ethanol and water to remove precipitant. The supernatant was further dialyzed against water through a dialysis membrane (Mw = 2 kDa) to remove small molecules. The pale-yellow BCDs were obtained via freeze-dry processing technology. As a contrast, pure CDs were synthesized according to the same experimental operation without BPEI.

Synthesis of Ru-BCDs Nanohybrid. The self-enhanced Ru-BCDs were synthesized through a cross-linking reaction between the carboxyl $Ru(dcbpy)_3^{2+}$ and the amines of BCDs. $Ru(dcbpy)_3^{2+}$ (11.13 mg) was added into a solution of EDC (25.60 mg) and NHS (9.17 mg) in H_2O (4.0 mL) to activate carboxyl groups. The mixture was ultrasonically treated to obtain a transparent solution and then stirred at room temperature for about 30 min. BCDs (20.0 mg) were dissolved in 4 mL of a H_2O/ethanol mixture solvent (1:1, v/v). The activated solution of $Ru(dcbpy)_3^{2+}$ and BCDs was mixed and stirred at room temperature for 24 h. The final solution was ultrafiltered (0.22 μm) to eliminate the large nanoparticles and further dialyzed against water to obtain an orange-red solution (Ru-BCDs).

Fabrication of the ECL Sensor. The GCE was polished with 0.05 μm alumina and ultrasonically cleaned in ultrapure water and ethanol before use. At first, 10 μL of the solution of Ru-BCDs was modified on the cleaned GCE. After the clean GCE was dried, 6 μL of CNN was dropped on it overnight in a light-proof drier. Then probe DNA (6 μL, 100 nM) was incubated on the GCE surface to react for 2 h at 4 °C and gently rinsed with ultrapure water. Next, 6 μL of 2 mM blocking reagent (AP) in PBS buffer was coated on the electrode to react for 1 h to cover the unbound binding sites.[32] Different concentrations of miR-133a were incubated with the modified electrode for 40 min at room temperature. After that, the electrode was rinsed using PBS to release the duplex DNA−RNA complex.

RESULTS AND DISCUSSION

Characterization of BCDs and Ru-BCDs. The as-prepared BCDs showed spherical morphology with high monodispersing property (Figure 2A). The average diameter

DOI: 10.1021/acs.analchem.9b03674
Anal. Chem. 2019, 91, 13237−13243

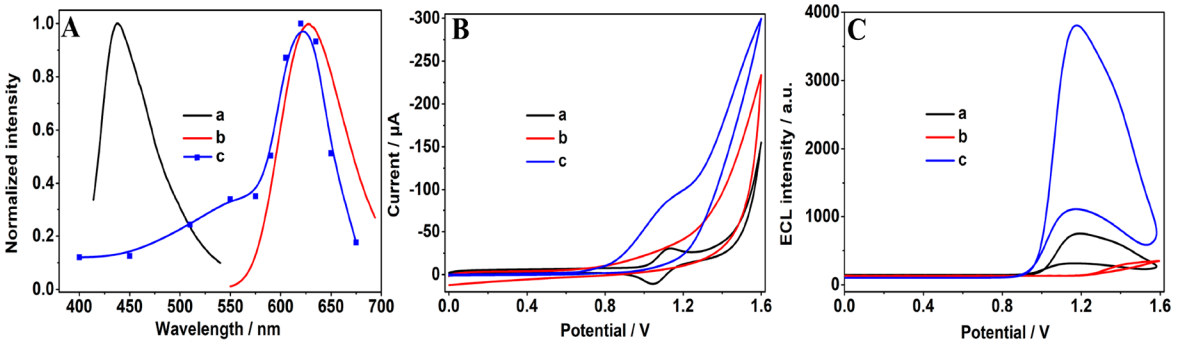

Figure 3. (A) Normalized fluorescence spectrum of (a) BCDs, (b) $Ru(dcbpy)_3^{2+}$, and (c) ECL spectra of Ru-BCDs/GCE. (B) CV and (C) ECL-potential curves of (a) $Ru(dcbpy)_3^{2+}$, (b) BCDs, and (c) Ru-BCDs-modified GCE, 6 μL of 0.1 mg/mL solution was dropped on the electrode surface. Electrolyte: 0.1 M PBS (pH 7.4). PMT: 400 V.

of the nanodots was determined to be 3.0 ± 0.4 nm (Figure 2A, inset). The high-resolution TEM image showed the lattice spacing of 0.21 nm (Figure 2B), which was consistent with the in-plane lattice spacing of graphene (100 facet).[33] The UV−visible absorption, fluorescence, and FT-IR spectra were used to characterize the physicochemical properties of BCDs. UV−visible absorption of BCDs showed two peaks centered at 248 nm (π–π^* transition of C═C) and 358 nm (n–π^* transition of C═O), while CA and BPEI did not have an obvious absorption band from 230 to 550 nm (Figure S1A, dotted line).[34] The solution of BCDs exhibited a blue color under ultraviolet light and a pale-yellow color under visible light (Figure S1A, inset). The fluorescence spectra showed a maximum excitation wavelength at 366 nm and a maximum emission wavelength at 449 nm (Figure S1A, solid line). The FT-IR spectrum of BCDs showed characteristic peaks of −NH− (3439 cm^{-1}, 1557 cm^{-1}), $-CH_2-$ (2954 cm^{-1}, 2849 cm^{-1}), and −CN− (1183 cm^{-1}), which were consistent with characteristic peaks of BPEI, but nearly no similar peak appeared for CA (Figure S1B).[35] The result indicated that primarily CA had the potential to be carbonized after microwave heating, while the BPEI remained stable. The abundant functional groups (amine group) on the surface of BCDs were greatly beneficial for the water solubility and the ability as a coreactant. Besides, a new peak of −CONH− (1704 cm^{-1}) indicated that BPEI was coated on the surface of BCDs through amide bonds. The above experimental results indicated the successful preparation of BPEI-coated CDs.

The Ru-BCDs particles were well-dispersed with the average diameter of 12.1 ± 1.4 nm (Figure 2C). Dynamic light scattering analysis showed the hydrodynamic size of BCDs and Ru-BCDs centered at about 4.19 nm and about 23.82 nm, respectively (Figure S2A,B). The incremental particle size was attributed to the cross-linking between one $Ru(dcbpy)_3^{2+}$ and multiple amine-rich BCDs. XPS measurements were carried out to analyze the surface elements of Ru-BCDs (Figure 2D). As anticipated, the characteristic peaks of O 1s (532 eV), Ru 3p (475 eV), N 1s (399 eV), and C 1s (284 eV) were presented in the XPS survey spectrum. In the deconvoluted high-resolution C 1s spectrum (Figure S3A), the three characteristic peaks of C−C sp^2 (284.5 eV), C−N/C−O (285.7 eV), and C═O (288.2 eV) indicated that Ru-BCDs contain abundant graphite structures and oxygen-containing groups.[36] The deconvoluted high-resolution Ru 3p spectrum showed a doublet at 462.3 and 484.8 eV (Figure S3B), which confirmed the presence of Ru(II) in the nanohybrid.[37] As shown in the FT-IR spectra (Figure 2E), Ru-BCDs showed stretching vibration peaks of $-CH_2-$ at 2976 and 2873 cm^{-1}, which was identical to BCDs. The peak component of −COOH (1721 cm^{-1}) dropped dramatically; meanwhile, two new vibrations peaks (amide I at 1653 cm^{-1}, amide II at 1565 cm^{-1}) appeared because of the formation of −CONH−. The UV−vis absorption spectrum of Ru-BCDs performed four absorption peaks at 248, 306, 354, and 473 nm (Figure 2F). Apparently, the peaks at 248 and 354 nm were the characteristic peaks of BCDs, while the peaks at 306 and 473 nm originated from $Ru(dcbpy)_3^{2+}$ with a slight red-shift. All the above evidence confirmed the covalent attachment between $Ru(dcbpy)_3^{2+}$ and BCDs.

ECL Performance of Ru-BCDs. The dual enhanced contribution of BCDs to the ECL of $Ru(dcbpy)_3^{2+}$ was first investigated in PBS buffer solution. As shown in Figure S4, alone $Ru(dcbpy)_3^{2+}$ and CDs showed very weak ECL emission because of the lack of coreactant (curves a and b). When adding CDs or BPEI to the $Ru(dcbpy)_3^{2+}$ solution (curves c and d), the ECL intensity was greatly increased because BPEI and CDs could act as the coreactants of $Ru(dcbpy)_3^{2+}$ as reported previously.[11,37] Surprisingly, when BCDs were added into the $Ru(dcbpy)_3^{2+}$ solution (curve e), the ECL intensity was further increased to 2.7-fold or 2.0-fold that of CDs or BPEI as coreactant, respectively. These results demonstrated the high enhancement efficiency of BCDs to the ECL of $Ru(dcbpy)_3^{2+}$, which was attributable to the dual enhanced contribution of BCDs from CDs and BPEI. Moreover, the fluorescence and ECL spectrum were recorded to confirm the ECL emitter (Figure 3A). The fluorescence maximum emission wavelengths of BCDs and $Ru(dcbpy)_3^{2+}$ were centered at 434 and 627 nm, respectively. The ECL spectrum of the Ru-BCDs-modified electrode showed the maximum intensity at 622 nm, which was consistent with the fluorescence spectrum of $Ru(dcbpy)_3^{2+}$. The result indicated that the ECL emission of Ru-BCDs originated from Ru-$(dcbpy)_3^{2+}$ rather than BCDs. That is to say, the $Ru(dcbpy)_3^{2+}$ acted as luminophore and BCDs served as self-coreactant in the Ru-BCDs nanohybrid.

The electrochemical and ECL behaviors of $Ru(dcbpy)_3^{2+}$, BCDs, and Ru-BCDs-modified GCE were investigated in detail. The pure $Ru(dcbpy)_3^{2+}$-modified electrode had a pair of typical redox peaks at 1.13 and 1.05 V (Figure 3B, curve a), while BCD-modified electrode does not show obvious redox peaks under the same condition. For Ru-BCDs/GCE, the oxidation peak at 1.13 V increased, and the reduction peak decreased dramatically, indicating the catalytic oxidation of $Ru(dcbpy)_3^{2+}$ (curve c). As shown in Figure 3C, alone BCDs

DOI: 10.1021/acs.analchem.9b03674
Anal. Chem. 2019, 91, 13237−13243

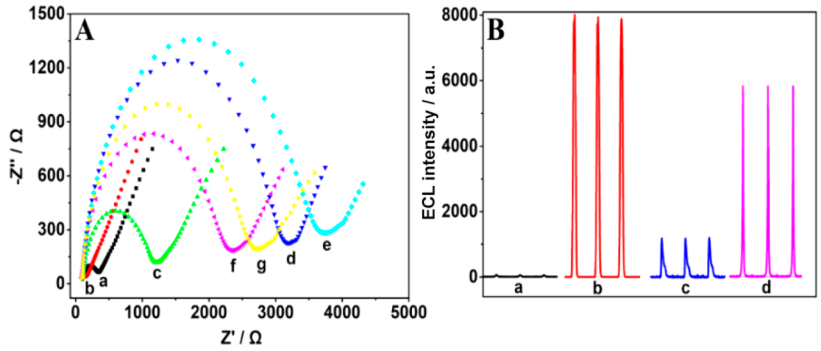

Figure 4. (A) EIS characterization of the biosensor. (a) Bare GCE, (b) Ru-BCDs/GCE, (c) CNN/Ru-BCDs/GCE, (d) probe DNA/CNN/Ru-BCDs/GCE, (e) AP/probe DNA/CNN/Ru-BCDs/GCE, (f) 100 pM target RNA/AP/probe DNA/CNN/Ru-BCDs/GCE, and (g) 50 pM target RNA/AP/probe DNA/CNN/Ru-BCDs/GCE. Electrolyte: 5 mM $[Fe(CN)_6]^{3-/4-}$ containing 0.1 M KCl. (B) ECL intensities of (a) bare GCE, (b) CNN/Ru-BCDs/GCE, (c) 100 nM probe DNA/CNN/Ru-BCDs/GCE, and (d) 100 pM target RNA/AP/probe DNA/CNN/Ru-BCDs/GCE.

(curve a) and $Ru(dcbpy)_3^{2+}$ (curve b) modified electrodes showed very weak ECL emission, indicating that alone BCDs or $Ru(dcbpy)_3^{2+}$ was not a suitable ECL illuminant in this anodic ECL system without coreactant. However, the Ru-BCDs-modified GCE exhibited a strong ECL signal rising at 0.86 V and peaking at 1.15 V without additional coreactant (curve c), which was ascribed to the efficient intramolecular electron transfer with short electron-transfer path and minor energy loss.[38] The results proved that Ru-BCDs could be used as a strong self-enhanced ECL probe.

The ECL mechanism of self-enhanced Ru-BCDs was summarized as follows and includes the benzylic alcohol oxidation mechanism of CDs (eqs 1−4)[38] and the amine oxidation mechanism of BPEI (eqs 5−8).[6] With the potential positive scanning, the components in $Ru_{(II)}$-BCDs are oxidized to form $Ru_{(III)}$-BCDs(-C_6H_5CHOH-)$^{\bullet+}$ and/or $Ru_{(III)}$-BCDs-(BPEI)$^{\bullet+}$ (eqs 1 and/or 5), which further deprotonate to produce $Ru_{(III)}$-BCDs(-C_6H_5COH-)$^{\bullet}$ and/or $Ru_{(III)}$-BCDs-(BPEI)$^{\bullet}$ intermediate (eqs 2 and/or 6). Then, the strong oxidant intermediates change to the excited state $Ru_{(II)}^*$-BCDs(-C_6H_5CO-) and $Ru_{(II)}^*$-BCDs(BPEI) via the intramolecular electron and energy transfer (eqs 3 and 7). Finally, the excited state molecules return to the ground state accompanied by strong ECL emission (eqs 4 and 8).

$$Ru_{(II)}\text{-BCDs}(\text{-}C_6H_5CHOH\text{-}) - 2e^- \rightarrow Ru_{(III)}\text{-BCDs}(\text{-}C_6H_5CHOH\text{-})^{\bullet+} \quad (1)$$

$$Ru_{(III)}\text{-BCDs}(\text{-}C_6H_5CHOH\text{-})^{\bullet+} \rightarrow Ru_{(III)}\text{-BCDs}(\text{-}C_6H_5COH\text{-})^{\bullet} + H^+ \quad (2)$$

$$Ru_{(III)}\text{-BCDs}(\text{-}C_6H_5COH)^{\bullet} \rightarrow Ru_{(II)}^*\text{-BCDs}(\text{-}C_6H_5CO\text{-}) + H^+ \quad (3)$$

$$Ru_{(II)}^*\text{-BCDs}(\text{-}C_6H_5CO\text{-}) \rightarrow Ru_{(II)}\text{-BCDs}(\text{-}C_6H_5CO\text{-}) + hv \quad (4)$$

and/or

$$Ru_{(II)}\text{-BCDs(BPEI)} - 2e^- \rightarrow Ru_{(III)}\text{-BCDs(BPEI)}^{\bullet+} \quad (5)$$

$$Ru_{(III)}\text{-BCDs(BPEI)}^{\bullet+} \rightarrow Ru_{(III)}\text{-BCDs(BPEI)}^{\bullet} + H^+ \quad (6)$$

$$Ru_{(III)}\text{-BCDs(BPEI)}^{\bullet} \rightarrow Ru_{(II)}^*\text{-BCDs(BPEI)} \quad (7)$$

$$Ru_{(II)}^*\text{-BCDs(BPEI)} \rightarrow Ru(II)\text{-BCDs(BPEI)} + hv \quad (8)$$

Although Ru-BCDs-modified GCE showed extremely strong ECL responses, the ECL intensity was not stable (RSD = 13.6%) because of the high water dispersibility (Figure S5A). Considering the superb film-forming property of CNN, CNN was dropped onto the Ru-BCDs/GCE to efficiently prevent the dissolution of Ru-BCDs. The prepared CNN showed the planar structure with a dimension of 10−180 nm and a thickness of around 3.0 nm (Figure S6, and the detailed characterization was shown in Supporting Information). Finally, a stable ECL signal was obtained with the RSD of 1.25% (Figure S5B). The strong and stable ECL response was beneficial to the ECL detection.

Characterization of the Biosensor. The electron-transfer resistance (R_{et}) of the EIS experiment could be used to study the practicability of the biosensor. As shown in Figure 4A, the bare GCE had a small R_{et} (curve a). After the immobilization of Ru-BCDs onto the GCE surface, the diameter of the semicircle decreased (curve b), suggesting Ru-BCDs/GCE had a low R_{et}. When CNN was coated on the electrode surface (curve c), a curve with a big semicircle was obtained because CNN exhibited poor conductivity. The R_{et} further increased when probe DNA was anchored onto the electrode (curve d) because of the repulsive interaction between the negatively charged probe DNA and $[Fe(CN)_6]^{3-/4-}$ probe. Subsequently, the modification of blocking reagent further resulted in the increase of R_{et} (curve e).[23] Finally, when the different concentrations of target RNA were dropped (curves f and g), the R_{et} values decreased, and a higher concentration of target RNA caused a larger decrease of R_{et}. These results implied that the hybridized products formed between probe DNA and target RNA fell off from the electrode surface, indicating the sensing interface was fabricated successfully.

The ECL signals of the stepwise fabrication were also evaluated to character the biosensor (Figure 4B). The Ru-BCDs-modified electrode showed a very strong ECL response (curve b) compared with the bare GCE (curve a). However, the ECL intensity showed an obvious decrease after probe DNA was treated (curve c) because the ferrocenes at both ends of probe DNA could quench the ECL response of Ru-BCDs. Excitingly, the ECL intensity would recover after target RNA was added because the probe DNA/target RNA duplex

DOI: 10.1021/acs.analchem.9b03674
Anal. Chem. 2019, 91, 13237−13243

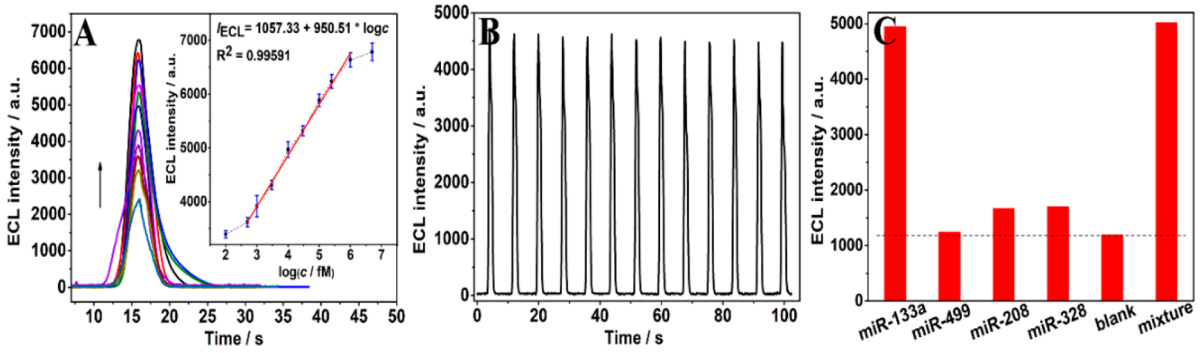

Figure 5. (A) ECL signals of proposed sensor to different concentrations of miR-133a (0, 100 fM, 500 fM, 1 pM, 3 pM, 10 pM, 30 pM, 100 pM, 500 pM, 1 nM, and 5 nM in the direction of the arrow). Inset was linear relationship between the ECL response and the logarithm concentration of miR-133a. (B) The ECL responses of biosensor during a continuous potential scan from 0 to 1.6 V in 0.1 M PBS (pH 7.4). (C) Selectivity of the biosensor for miR-133a (10 pM) against other AMI-related miRNAs (50 pM).

fell off from the GCE surface (curve d). The results confirmed the feasibility of the biosensor.

Analytical Performance of the Biosensor. Under the optimum conditions of 0.01 mg/mL CNN, 100 nM probe DNA, 2 h probe DNA incubation time, and 40 min target RNA incubation time (details are displayed in Figure S7 of Supporting Information), the analytical performance of the biosensor was evaluated through monitoring the ECL response to different concentrations of miR-133a. With the increase of miR-133a concentration, more DNA probes were released from the electrode surface, resulting in increased ECL signal (Figure 5A). The ECL signal showed a linear relationship with miR-133a concentration from 500 fM to 1 nM (Figure 5A, inset). Once miR-133a concentration was less than 500 fM or more than 1 nM, the ECL intensity would deviate from the linear calibration curve. The linear equation was I_{ECL} = 1057.33 + 950.51log$C_{miR\text{-}133a}$, and the detection limit was 0.06 M (S/N = 3). The proposed biosensor exhibited a higher or comparable sensitivity compared with other label-free biosensors for nucleic acid detection (Table S1).

The ECL intensity of repetitive cyclic voltammetry for 13 cycles was recorded (Figure 5B). The relative standard deviation (RSD) of 13 ECL signals was 1.68%, which showed the high stability and reproducibility of the designed biosensor. The interference experiments were performed to assess the selectivity of ECL sensor. Other AMI-related miRNAs[39] including miR-499, miR-208, and miR-328, were chosen as interference RNAs. As shown in Figure 5C, the mixture of miR-133a and nonspecific miRNAs showed identical ECL response to the pure miR-133a, and nonspecific miRNAs showed similar response comparing with the blank sample, indicating the great specificity of this sensing platform.

The recovery experiment was carried out by standard adding miR-133a to 1% or 5% real human serum in order to estimate the practical application of the proposed biosensor. The recoveries were calculated from 93% to 110.6%, and all RSDs after three times of detection were not more than 5%, indicating the excellent potential of the biosensor to miR-133a detection in real serum samples.

CONCLUSIONS

Herein, a self-enhanced ECL nanohybrid (Ru-BCDs) was prepared by covalently linking BCDs and $Ru(dcbpy)_3^{2+}$, which exhibited strong and stable ECL signal without extra coreactant due to an efficient intramolecular electron transfer process. BPEI and carbon dots in BCDs were regarded as dual enhanced contributors to the ECL performance of Ru-BCDs. Moreover, a label-free biosensor was proposed for the detection of miR-133a-based self-enhanced Ru-BCDs and the affinity changes of CNN to single-stranded DNA and double helix DNA. Our proposed biosensor possessed satisfying stability and selectivity, resulting in a simple and fast detection of target RNA in diluted human serum. This work provided a new method for preparing a self-enhanced ECL luminophore, which would find extensive applications in clinical and biochemical analysis.

ASSOCIATED CONTENT

Supporting Information

The Supporting Information is available free of charge on the ACS Publications website at DOI: 10.1021/acs.analchem.9b03674.

Apparatus; UV−vis absorption spectra, fluorescence, and FT-IR spectra of CA, BPEI, and BCDs; DLS analysis of BCDs and Ru-BCDs; deconvoluted high-resolution XPS spectra of C 1s and Ru 3p; ECL-potential curves in PBS; ECL responses of Ru-BCDs/GCE and CNN/Ru-BCDs/GCE; characterization of CNN; optimization of the detection conditions; comparison of the performance of the proposed biosensor with the reported label-free nucleic acid biosensors; analytical performance of the proposed biosensor for the detection of miR-133a in human serum samples (PDF)

AUTHOR INFORMATION

Corresponding Authors

*E-mail: xryang@ciac.ac.cn. Tel.: +86 431 85262056; Fax: +86 431 85689278.

*E-mail: huangjs@ciac.ac.cn. Tel: +86 431 85262964. Fax: +86 431 85689278.

ORCID

Xiurong Yang: 0000-0003-0021-5135

Author Contributions

The manuscript was written through contributions of all authors.

Notes

The authors declare no competing financial interest.

DOI: 10.1021/acs.analchem.9b03674
Anal. Chem. 2019, 91, 13237−13243

■ ACKNOWLEDGMENTS

This work was supported by the National Key Research and Development Program of China (2016YFA0201301), the National Natural Science Foundation of China (no. 21435005, 21627808 and 21721003), Key Research Program of Frontier Sciences, CAS (QYZDY-SSW-SLH019), and the Development Project of Science and Technology of Jilin Province (No. 20170101195JC).

■ REFERENCES

(1) Wang, H.; Yuan, Y.; Zhuo, Y.; Chai, Y. Q.; Yuan, R. *Anal. Chem.* **2016**, *88*, 5797−5803.
(2) Zhang, M.; Hai, H.; Zhou, F. Y.; Zhong, J. C.; Li, J. P. *Chin. J. Anal. Chem.* **2018**, *46*, 203−209.
(3) Feng, D. F.; Tan, X. C.; Wu, Y. Y.; Ai, C. H.; Luo, Y. N.; Chen, Q. Y.; Han, H. Y. *Biosens. Bioelectron.* **2019**, *129*, 100−106.
(4) Yu, Y. Q.; Wang, J. P.; Zhao, M.; Hong, L. R.; Chai, Y. Q.; Yuan, R.; Zhuo, Y. *Biosens. Bioelectron.* **2016**, *77*, 442−450.
(5) Zhang, L.; He, Y.; Wang, H. J.; Yuan, Y. L.; Yuan, R.; Chai, Y. Q. *Biosens. Bioelectron.* **2015**, *74*, 924−930.
(6) Wang, H. J.; Yuan, Y. L.; Zhuo, Y.; Chai, Y. Q.; Yuan, R. *Anal. Chem.* **2016**, *88*, 2258−2265.
(7) Wang, H. J.; He, Y.; Chai, Y. Q.; Yuan, R. *Nanoscale* **2014**, *6*, 10316−10322.
(8) Sun, S. G.; Yang, Y.; Liu, F. Y.; Fan, J. L.; Peng, X. J.; Kehr, J.; Sun, L. C. *Dalton. Trans.* **2009**, *7969*, 7969−7974.
(9) Sun, S. G.; Yang, Y.; Liu, F. Y.; Fan, J. L.; Kehr, J.; Sun, L. C.; Peng, X. J. *Dalton. Trans.* **2010**, *39*, 8626−8630.
(10) Zhuo, cY.; Liao, N.; Chai, Y. Q.; Gui, G. F.; Zhao, M.; Han, J.; Xiang, Y.; Yuan, R. *Anal. Chem.* **2014**, *86*, 1053−1060.
(11) Gui, G. F.; Zhuo, Y.; Chai, Y. Q.; Xiang, Y.; Yuan, R. *Anal. Chem.* **2014**, *86*, 5873−5880.
(12) Liang, W. B.; Zhuo, Y.; Xiong, C. Y.; Zheng, Y. N.; Chai, Y. Q.; Yuan, R. *Anal. Chem.* **2015**, *87*, 12363−12371.
(13) Xiong, C. Y.; Liang, W. B.; Zheng, Y. N.; Zhuo, Y.; Chai, Y. Q.; Yuan, R. *Anal. Chem.* **2017**, *89*, 3222−3227.
(14) Li, L. B.; Liu, D.; Mao, H. P.; You, T. Y. *Biosens. Bioelectron.* **2017**, *89*, 489−495.
(15) Xu, Z. H.; Yu, J. G.; Liu, G. *Sens. Actuators, B* **2013**, *181*, 209−214.
(16) Li, L. B.; Yu, B.; Zhang, X. P.; You, T. Y. *Anal. Chim. Acta* **2015**, *895*, 104−111.
(17) Luo, L. J.; Li, L. B.; Xu, X. X.; Liu, D.; Li, J. Y.; Wang, K.; You, T. Y. *RSC Adv.* **2017**, *7*, 50634−50642.
(18) Qi, B. P.; Zhang, X. R.; Shang, B. B.; Xiang, D. S.; Qu, W. Y.; Zhang, S. H. *Carbon* **2017**, *121*, 72−78.
(19) Carrara, S.; Arcudi, F.; Prato, M.; De Cola, L. *Angew. Chem., Int. Ed.* **2017**, *56*, 4757−4761.
(20) Chen, X. Q.; Liu, Y.; Ma, Q. *J. Mater. Chem. C* **2018**, *6*, 942−959.
(21) Han, Z. L.; Shu, J. N.; Jiang, Q. S.; Cui, H. *Anal. Chem.* **2018**, *90*, 6064−6607.
(22) He, S. J.; Song, B.; Li, D.; Zhu, C. F.; Qi, W. P.; Wen, Y. Q.; Wang, L. H.; Song, S. P.; Fang, H. P.; Fan, C. H. *Adv. Funct. Mater.* **2010**, *20*, 453−459.
(23) Xu, H. F.; Liang, S. J.; Zhu, X.; Wu, X. Q.; Dong, Y. Q.; Wu, H. S.; Zhang, W. X.; Chi, Y. W. *Biosens. Bioelectron.* **2017**, *92*, 695−701.
(24) Tan, C. L.; Yu, P.; Hu, Y. L.; Chen, J. Z.; Huang, Y.; Cai, Y. Q.; Luo, Z. M.; Li, B.; Lu, Q. P.; Wang, L. H.; Liu, Z.; Zhang, H. *J. Am. Chem. Soc.* **2015**, *137*, 10430−10436.
(25) Liu, J.; Zheng, T. T.; Tian, Y. *Angew. Chem., Int. Ed.* **2019**, *58*, 7757−7761.
(26) Zhou, H.; Peng, J. B.; Qiu, X. L.; Gao, Y. S.; Lu, L. M.; Wang, W. M. *J. Mater. Chem. B* **2017**, *5*, 7426−7432.
(27) Ji, J. J.; Wen, J.; Shen, Y. F.; Lv, Y. Q.; Chen, Y. L.; Liu, S. Q.; Ma, H. B.; Zhang, Y. J. *J. Am. Chem. Soc.* **2017**, *139*, 11698−11701.
(28) Zhang, X. D.; Xie, X.; Wang, H.; Zhang, J. J.; Pan, B. C.; Xie, Y. *J. Am. Chem. Soc.* **2013**, *135*, 18−21.
(29) Liao, X. J.; Wang, Q. B.; Ju, H. X. *Chem. Commun.* **2014**, *50*, 13604−13607.
(30) Feng, Y. Q.; Wang, Q. B.; Lei, J. P.; Ju, H. X. *Biosens. Bioelectron.* **2015**, *73*, 7−12.
(31) Chang, Y. Y.; Li, M. Y.; Wu, Z. Y.; Zhuo, Y.; Chai, Y. Q.; Xiao, Q.; Yuan, R. *Anal. Chem.* **2018**, *90*, 8241−8247.
(32) Feng, L. Y.; Wu, L.; Wang, J. S.; Ren, J. S.; Miyoshi, D.; Sugimoto, N.; Qu, X. *Adv. Mater.* **2012**, *24*, 125−131.
(33) Cheng, J.; Wang, C. F.; Zhang, Y.; Yang, S. Y.; Chen, S. *RSC Adv.* **2016**, *6*, 37189−37194.
(34) Liu, Y.; Han, S. Q. *New J. Chem.* **2018**, *42*, 388−394.
(35) Dong, Y. Q.; Wang, R. X.; Li, H.; Shao, J. W.; Chi, Y. W.; Lin, X. M.; Chen, G. N. *Carbon* **2012**, *50*, 2810−2815.
(36) Dong, Y. Q.; Lin, J. P.; Chen, Y. M.; Fu, F. F.; Chi, Y. W.; Chen, G. N. *Nanoscale* **2014**, *6*, 7410−7415.
(37) Long, Y. M.; Bao, L.; Zhao, J. Y.; Zhang, Z. L.; Pang, D. W. *Anal. Chem.* **2014**, *86*, 7224−7228.
(38) Chen, A. Y.; Zhao, M.; Zhuo, Y.; Chai, Y. Q.; Yuan, R. *Anal. Chem.* **2017**, *89*, 9232−9238.
(39) Sun, Y. D.; Li, T. *Anal. Chem.* **2018**, *90*, 11614−11621.

DOI: 10.1021/acs.analchem.9b03674
Anal. Chem. 2019, 91, 13237−13243